J Nanopart Res (2013) 15:1866
DOI 10.1007/s11051-013-1866-0

RESEARCH PAPER

The use of the grey-Taguchi method for the optimization of a silicon nanowires array synthesized using electroless Ag-assisted etching

Ai-Huei Chiou · Wen-Fa Wu · Ding-Yeng Chen · Chun-Yao Hsu

Received: 11 May 2012 / Accepted: 15 July 2013 / Published online: 9 August 2013

Abstract A simple and convenient method for the production of silicon nanowires (SiNWs) that are single crystalline, well aligned and which have large area is direct synthesis onto p-type (100) silicon (Si) wafers, using electroless Ag-assisted etching, in which Ag is both the oxidant and the catalyst. This study proposes a method for the optimization of the etching process parameters for SiNW arrays with multiple performance characteristics, using grey-Taguchi analysis. The effect of the etching process parameters (etching time, solution ($AgNO_3$/HF) temperature, silver nitrate ($AgNO_3$) concentration and hydrogen fluoride (HF) concentration) on the length, diameter, structure, and morphology of the SiNW arrays were studied. In the confirmation runs, grey relational analysis shows that the length of the SiNW arrays is increased from 15.80 to 23.07 μm, and the diameter is decreased from 76.77 to 66.65 nm. Further, the linear relationship for the SiNW arrays can be adjusted by increasing the etching time (from 15 to 45 min) and the solution temperature (from 25 to 75 °C). The axial orientation of the SiNWs is determined to be along the [001] direction, which is the same as that of the initial Si wafer. The large area SiNW arrays have potential applications in interconnect, bio-technology and opto-electronic devices.

Keywords Silicon nanowires arrays · Electroless Ag-assisted etching · Grey-Taguchi method

A.-H. Chiou
Department of Mechanical Engineering, National Chiao Tung University, Hsinchu, Taiwan, ROC

W.-F. Wu
National Nano Device Laboratories, Hsinchu, Taiwan, ROC

D.-Y. Chen (✉)
Department of Mechanical Engineering, Hwa Hsia Institute of Technology, Taipei 23568, Taiwan, ROC
e-mail: dnc@cc.hwh.edu.tw

C.-Y. Hsu (✉)
Department of Mechanical Engineering, Lunghwa University of Science and Technology, Guishan, Taiwan, ROC
e-mail: cyhsu@mail.lhu.edu.tw

Introduction

Following the discovery of carbon nanotubes, by Iijima, in 1991, one-dimensional (1D) nanowires have been widely studied, because of their excellent physical, chemical, magnetic, optical, mechanical, and other properties. Of the many 1D materials, silicon nanowires (SiNWs) are important because of their semiconducting properties. SiNW-based nanodevices have many applications (Peng et al. 2004; Ma et al. 2003; Teo and Sun 2007; He et al. 2010; Shao et al. 2010; Peng and Lee 2011; Bandaru and Pichanusakorn

2010), such as field-effect transistors, biological sensors and integrated logic circuits, have all been demonstrated. There are various methods for the synthesis of 1D SiNWs arrays, including chemical, electrochemical, and physical deposition techniques. However, some methods, such as catalytic growth using the vapor–liquid–solid method and metal organic-chemical vapor deposition are expensive and energy-consuming processes, since they require extreme conditions for operation.

Recently, well-aligned SiNW arrays has been widely demonstrated (Peng et al. 2003, 2009a, b, c; Peng and Zhu 2003), fabricated using facile-assisted metal etching. This method of fabricating SiNW arrays has many advantages, including low cost and large surface area. It also allows control of the conductivity, which allows applications in electronic-related devices such as field-effect transistors, lithium ion batteries, or electrochemical biosensors. There are, however, problems associated with the repeatable and controllable preparation of SiNW arrays from substrates with defined type, orientation, size, doping level and improved conduction. When the diameter is less than 150 nm, the surface charge sensitivity of the SiNWs is good (Elfström et al. 2007). The geometric control of fabricated SiNWs, including their length, size and orientation, render them suitable to many potential applications. This paper studies the effect of the electroless Ag-assisted etching (EAAE) process parameters on the length, diameter, structure, and morphology of SiNW arrays.

Taguchi methods are a system of cost-driven quality engineering that emphasizes the effective application of engineering strategies rather than advanced statistical techniques. They have been widely applied in many engineering optimization problems, such as Cu wires (Su and Yeh 2011), Ag chromate nanoparticles (Alamdari et al. 2010), and others (Liu et al. 2007; Kim et al. 2007). However, no studies have considered the complicated inter-relationships between multiple performance characteristics to synthesis SiNW arrays by grey-Taguchi method. Therefore, this study aims to provide a method for the optimization of the etching process parameters for SiNW arrays with multiple performance characteristics, using grey-Taguchi analysis.

The Taguchi method is used for the experiment and a generic signal-to-noise (S/N) ratio is used to quantify the current variation (Taguchi 1990). This method seeks to improve product or process quality by reducing the mean squared deviation. Depending on the particular type of characteristics involved, different S/N ratios may be applicable, including "the lower the better" (LB), or "the higher the better" (HB). The S/N ratios are calculated using the following equations (Hsu and Tsang 2008):

The higher the better (maximize):

$$S/N = -10\log\left(\frac{1}{n}\sum_{i=1}^{n}\frac{1}{y_i^2}\right) \tag{1}$$

The lower the better (minimize):

$$S/N = -10\log\left(\frac{1}{n}\sum_{i=1}^{n}y_i^2\right) \tag{2}$$

where n is the number of observations and y is the observed data; the *S/N* ratio is expressed using a decibel scale (dB).

An analysis of variance (ANOVA) is performed to determine which EAAE process parameters are statistically significant. The *S/N* ratio and ANOVA analyses allow the prediction of the optimal combination of process parameters (Chen and Hsu 2008). A confirmation experiment is then conducted to verify the optimal process parameters determined from the parameter design. An ANOVA and an *F*-test are used to analyze the experimental data, as (Taguchi 1990):

$$S_{\mathrm{m}} = \frac{\left(\sum \eta_{\mathrm{i}}\right)^2}{J}, \quad S_{\mathrm{T}} = \sum {\eta_{\mathrm{i}}}^2 - S_{\mathrm{m}} \tag{3}$$

$$S_{\mathrm{A}} = \frac{\left(\sum \eta_{\mathrm{Ai}}^2\right)^2}{N} - S_{\mathrm{m}}, \quad S_{\mathrm{E}} = S_{\mathrm{T}} - \sum S_{\mathrm{A}} \tag{4}$$

$$V_{\mathrm{A}} = \frac{S_{\mathrm{A}}}{f_{\mathrm{A}}}, \quad F_{\mathrm{Ao}} = \frac{V_{\mathrm{A}}}{V_{\mathrm{E}}} \tag{5}$$

where S_{T} is the sum of squares due to the total variation, S_{m} is the sum of squares due to the means, S_{A} is the sum of squares due to parameter A (A represents etching time, solution temperature, silver nitrate ($AgNO_3$) concentration and hydrogen fluoride (HF) concentration, respectively), S_{E} is the sum of squares due to error, η_{i} is the η value of each experiment ($i = 1,\ldots,9$), J is the number of experiments in the orthogonal array (in this work, $J = 9$), η_{Ai} is the sum of the ith level of parameter A ($i = 1, 2, 3$), N is the repeating number of each level of parameter A, f_{A} is the degree of freedom of parameter A and V_{A} is the variance of parameter A.

Grey relational analysis can be used to effectively determine the complicated interrelationships between multiple performance characteristics. The grey relational coefficient is (Deng 1989):

$$r(x_0(k), x_i(k)) = \frac{\min_i \min_k |x_0(k) - x_i(k)| + \zeta \max_i \max_k |x_0(k) - x_i(k)|}{|x_0(k) - x_i(k)| + \zeta \max_i \max_k |x_0(k) - x_i(k)|} \quad (6)$$

where $x_i(k)$ is the normalized value of the kth performance characteristic in the ith experiment and ζ is the distinguishing coefficient ($\zeta \in [0, 1]$). The value of ζ can be adjusted in accordance with actual system requirements. The EAAE process parameters used in this paper are of equal weighting, so ζ is 0.5.

The grey relational grade is a weighting-sum of the grey relational coefficient. It is defined as follows (Deng 1990):

$$r(x_0, x_i) = \frac{1}{n} \sum_{k=1}^{n} r(r_0(k), x_i(k)) \quad (7)$$

where n is the number of performance characteristics.

Grey relational analysis, which is based on the grey system theory, can be used to determine the complicated inter-relationships between multiple performance characteristics. For the grey relational analysis, the experimental results for the length and diameter of the SiNWs are first normalized in the range between 0 and 1, which is termed, grey relational generation. Using the grey relational analysis and the statistical analysis of variance (ANOVA), the optimal combination of parameters for the etching of SiNW arrays can be predicted.

Experimental procedures

This study used 6-inch p-type (100) orientated silicon (Si) wafers with resistivity of 15–25 Ω cm for the substrate. In order to remove chemical impurities and particles, the wafers were cleaned using a standard Radio Corporation of American cleaning process (Kern and Puotinen 1970). In this procedure, a simple and convenient chemical method was used to synthesize SiNW arrays on p-type (100) orientated single-crystal Si wafers by EAAE. The Si substrates were cut into 1.5×1.5 cm^2 and cleaned with isopropyl alcohol, acetone, and distilled water. The SiNW arrays were then synthesized in a HF solution containing an $AgNO_3$ system. The as-prepared samples were immersed in HNO_3 solution for a few minutes, rinsed with de-ionized water, and dried in nitrogen. In order to remove oxide, the samples were dipped in 10 % HF solution.

In order to observe the effect of the EAAE process parameters on the fabricated SiNWs, four factors, each at three levels, were monitored: namely, an L_9 (3^4, with four columns and nine rows) orthogonal array was employed. Table 1 shows the factor and level settings for the EAAE parameters used for the SiNW arrays. The experiments were repeated twice.

The surface morphology of the SiNWs array was determined using field-emission scanning electron microscopy (FE-SEM, JEOL JSM-6500F) and transmission electron microscopy (TEM, JEM 2010F). The crystal structure of the SiNWs was evaluated using X-ray diffraction (Rigaku-2000 X-ray Generator.), using Cu Kα radiation with an angle of incidence of 1°. The incident angle scans from 20 to 90° show most of the characteristic peaks of the samples. The scanning rate was 5 degree/min. Raman spectroscopy is used to analyze the structure of many materials. This technique is highly sensitive to disorder on surfaces and measures the optical skin depth. Raman spectroscopy (Raman, Renishaw 2000) using a 17 mW He–Ne laser operating at 632.8 nm was utilized to examine the information between the crystallization and the atomic bands of the single-crystal SiNW arrays. The local atomic environment and bonding configuration of the samples were determined using Fourier transform infrared spectroscopy (FTIR).

Table 1 Factor settings and levels for the electroless Ag-assisted etching (EAAE) of SiNW arrays

Substrate		Silicon		
Type		*P* (1 0 0)		
Resistivity		15–25 Ω cm		
Base pressure		Normal pressure		
Symbol	Control factors	1	2	3
A	Etching time (min)	30	45	60
B	Solution temperature (°C)	25	50	75
C	$AgNO_3$ concentration (M)	0.02	0.06	0.12
D	HF (49 %) concentration (M)	4.6	9.2	13.8

Results and discussion

Control of the length of SiNW arrays

Table 2 shows the experimental results for the lengths of the SiNW arrays and the corresponding S/N ratios. Table 3 lists the ANOVA results for the lengths of the SiNW arrays. The variable that most affects the SiNW array length is the HF concentration ($P = 55.63$ %). The reason why concentration is very important reactions is explained by the collision theory of chemical reactions, which states that molecules must collide in order to react together. The frequency of the molecular collisions increases, as the concentration of the reactants increases, so a higher HF concentration (Table 3) results in an increased growth of the SiNW arrays, because the HF is better able to dissolve oxides. Figure 1 shows the top and side view SEM images of the SiNW arrays, for the experimental conditions, Nos. 1, 2, and 3 (HF concentration increases from 9.2 to 13.8 M). The length of the SiNWs is 1.59, 9.31, and 16.43 μm, respectively. It is apparent that the SiNWs etched with HF of lower concentration are isolated and, as the concentration of HF increases, the tips of the SiNWs congregate together.

The X-ray diffraction patterns for the SiNW arrays, no's 1–9 of the L_9 orthogonal array, are shown in Fig. 2. It is clear that all of the SiNW array peaks at 29.4 and 69.4° are attributable to (111) and (400) Si planes, respectively. For SiNW array no. 8 ($A_3B_2C_1D_3$), in the orthogonal array, the diffraction peaks are sharper and their full widths at half maximum (FWHM) are narrower. This demonstrates that the crystalline quality is improved.

Control of the diameter of SINW arrays

Figure 3 shows the diameter of SiNW arrays according to the statistics method. Table 4 shows the experimental results for the diameter and the corresponding S/N ratios of the SiNW arrays (measured more than 30 times). Table 5 lists the results of the ANOVA for the diameter of the SiNW arrays. The variable that most affects the diameter of the SiNW

Table 2 S/N ratios of the lengths of the SiNW arrays

No.	Control factors				SiNWs length (μm)				S/N (dB) larger is better
	A	B	C	D	Y_1	Y_2	Y_3	Mean	
1	1	1	1	1	1.52	1.54	1.72	1.59 ± 0.11	4.01
2	1	2	2	2	9.28	9.12	9.52	9.31 ± 0.20	19.37
3	1	3	3	3	16.10	16.90	16.30	16.43 ± 0.42	24.31
4	2	1	2	3	11.20	11.00	11.30	11.17 ± 0.15	20.96
5	2	2	3	1	1.50	1.39	0.50	1.13 ± 0.54	−2.19
6	2	3	1	2	13.10	13.40	13.20	13.23 ± 0.15	22.43
7	3	1	3	2	3.10	4.42	3.64	3.72 ± 0.66	11.14
8	3	2	1	3	15.08	16.01	15.60	15.56 ± 0.47	23.83
9	3	3	2	1	9.72	9.30	8.56	9.19 ± 0.59	19.23

A etching time, *B* solution temperature, *C* $AgNO_3$ concentration; *D* HF (49 %) concentration

Table 3 ANOVA results for the length of the SiNW arrays

Factor	S/N ratio (dB)			Degree of freedom	Sum of square	Variance	Contribution *P* (%)
	Level 1	Level 2	Level 3				
A	15.896	13.735	18.069	2	28.184	14.092	3.94
B	12.035	13.674	21.991	2	171.012	85.506	23.88
C	16.758	19.854	11.088	2	118.573	59.2865	16.55
D	7.018	17.648	23.033	2	398.486	199.243	55.63
Total				8	716.255		100

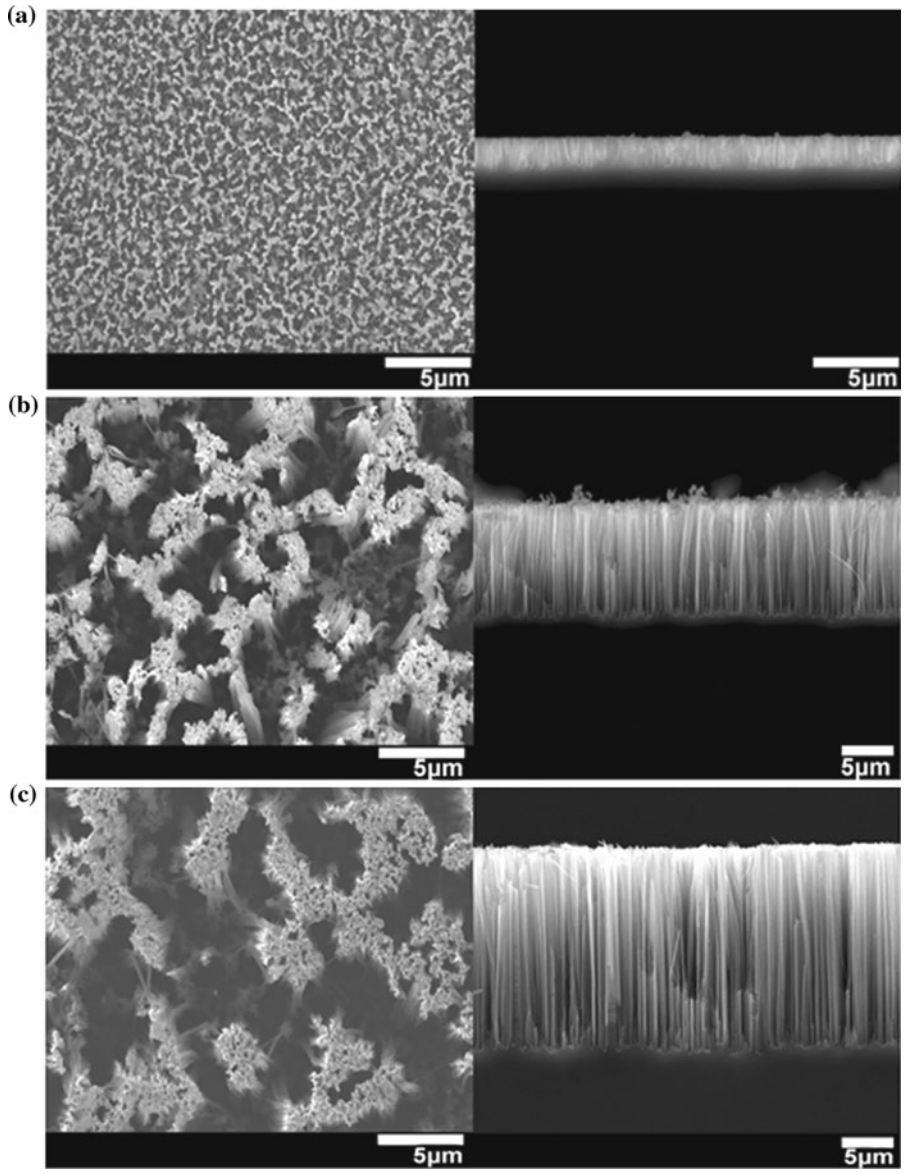

Fig. 1 The top and side view SEM images of the SiNW arrays, produced using the experimental conditions, Nos. 1, 2, and 3: **a** Experimental condition No. 1, at a HF concentration of 4.6 M and SiNW length = 1.59 μm, **b** experimental condition No. 2, at a HF concentration of 9.2 M and SiNW array length = 9.31 μm and **c** experimental condition No. 3, at a HF concentration of 13.8 M and SiNW array length = 16.43 μm

array is the $AgNO_3$ concentration. The diameter of the SiNW arrays can be controlled by adjusting the concentration of $AgNO_3$ in the etching solution. With a higher $AgNO_3$ concentration, the Ag nanoparticles are large. It can be seen that an increase in the concentration of $AgNO_3$ encourages the growth of Ag nanoparticles and results in an increase in particle size. This result is in agreement with the results of Peng et al. (2003).

Optimal EAAE parameters for the SiNW arrays, using the grey relationship

Using Eqs. (6) and (7), the grey relational grade for each experiment in the L_9 orthogonal array is shown in Table 6. This study obtained the optimal multiple performance characteristics for the SiNW arrays with orthogonal array parameters ($A_3B_2C_1D_3$) and the grey theory prediction design ($A_1B_3C_1D_3$). The confirmed

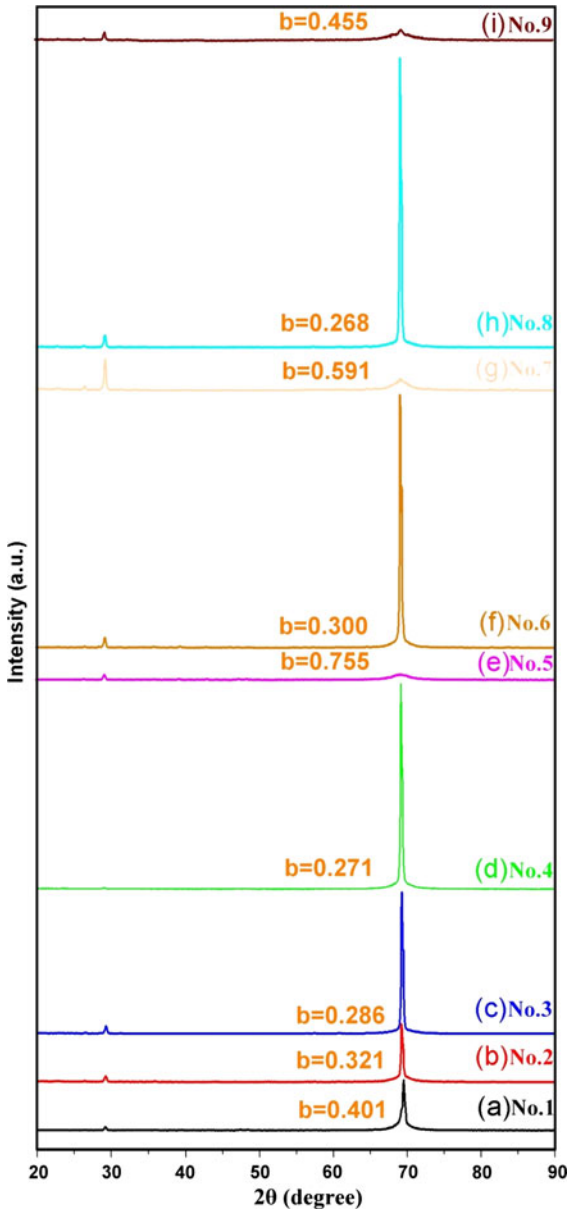

Fig. 2 XRD patterns for the SiNW arrays, for *numbers 1–9*, of the L_9 orthogonal array, (*b* full width at half maximum, FWHM)

experimental results for the optimum multiple performance characteristics for the SiNW arrays are shown in Table 7. A comparison of the grey theory prediction design with the orthogonal array parameters demonstrates that the diameter of the SiNW arrays is decreased from 76.77 to 66.65 nm and that the length is increased from 15.80 to 23.07 μm (Fig. 4).

Figure 5 shows the XRD diffraction patterns for the SiNW arrays. By applying grey theory prediction

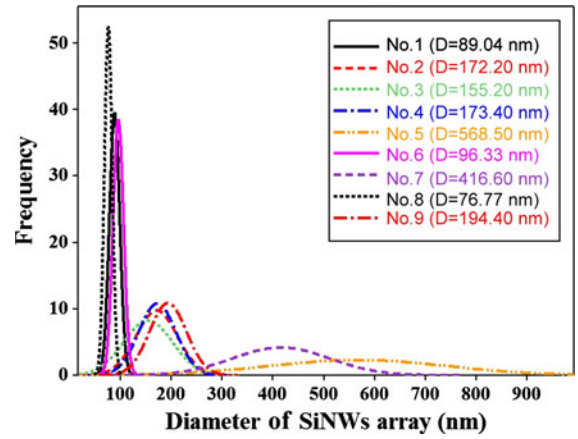

Fig. 3 Graph of the diameter of the SiNW arrays, for *numbers 1–9*, of the L_9 orthogonal array

design, it is seen that the intensity of the (400) diffraction peak is increased. According to Lyons et al. (2002), the axial direction of the SiNW arrays has a preferred orientation of (100). The FWHM decreases from 0.268 to 0.245, indicating that the crystallinity of the SiNW arrays can be improved.

The SiNW array characterization was performed using the combined TEM and EDX spectra from the grey theory prediction design sample. Figure 6a shows typical TEM images of as-synthesized SiNWs. The diameter of the SiNW arrays was observed to be in the range, 55–75 nm. Figure 6b shows the HRTEM images of the SiNWs, wherein the inter-planar spacing is estimated to be ~0.27 and ~0.31 nm, which corresponds to the (111) and (200) planes of Si, respectively. This result demonstrates that the axial direction of the SiNWs array is along the [100], which is the preferred p-type (100)-oriented orientation. This result is consistent with the XRD analysis (Fig. 5). The inset shows that the corresponding axial directions are characterized by selected area electron diffraction (SAED) patterns, indicating that the crystal is single crystalline. The elemental analysis demonstrates that SiNW arrays are Si and it shows only one peak comparable to Si, after the HNO_3 treatment, which indicates that Ag dendrites and Ag nanoparticles are removed completely, as shown in Fig. 6c.

Figure 7a shows the Raman spectra of a SiNW array, which show three distinct peaks at 297, 520, and 960 cm^{-1}, versus the first-order transverse optical phonon mode (TO), the second-order optical phonon mode (2TO) and the second-order transverse acoustic

Table 4 S/N ratios of the diameters of the SiNW arrays

No.	Control factors				SiNWs diameters (nm)										S/N (dB) small is better
	A	B	C	D	Y_1	Y_2	Y_3	Y_4	Y_5	Y_6	Y_7	Y_8	Y_9	Y_{10}	
1	1	1	1	1	79.68	112.5	79.67	84.37	97.10	86.7	94.35	86.77	80.35	88.9	−39.04
2	1	2	2	2	210.90	164.1	187.50	199.20	234.40	199.2	150.80	127.60	145.80	102.9	−44.94
3	1	3	3	3	156.20	109.4	265.60	127.00	171.90	187.5	167.40	115.90	101.80	148.9	−44.18
4	2	1	2	3	234.40	187.5	140.60	226.60	164.10	150.6	137.90	125.80	176.90	189.6	−44.95
5	2	2	3	1	326	731	270	500	600	658	489	580	753	778	−55.45
6	2	3	1	2	82.30	105.5	97.50	100.80	117.20	97.1	95.60	82.60	94.90	89.8	−39.72
7	3	1	3	2	375.00	421.9	562.50	328.10	515.60	278.7	515.50	310.50	450.70	407.8	−52.60
8	3	2	1	3	70.31	62.5	85.93	70.31	78.12	84.3	78.50	77.50	85.92	74.3	−37.74
9	3	3	2	1	168.00	160.0	192.00	216.00	162.00	250.0	144.00	195.00	209.00	248.0	−45.91

Table 5 ANOVA results for the diameter of the SiNW arrays

Factor	S/N ratio (dB)			Degree of freedom	Sum of square	Variance	Contribution *P* (%)
	Level 1	Level 2	Level 3				
A	−42.72	−46.71	−45.42	2	24.837	12.4185	8.74
B	−45.53	−46.04	−43.27	2	13.055	6.5275	4.59
C	−38.83	−45.27	−50.74	2	213.06	106.53	74.93
D	−46.80	−45.75	−42.29	2	33.391	16.6955	11.74
Total				8	284.343		100

Table 6 Grey relational grades and their order in the optimization process

No.	Grey relational grade	Order
1	0.6330	3
2	0.5310	6
3	0.6214	4
4	0.5436	5
5	0.4547	8
6	0.6921	2
7	0.3436	8
8	1.0000	1
9	0.5055	7

Table 7 Results of the confirmation experiment for multiple performance characteristics with an orthogonal array and the optimal predicted EAAE parameters

Level	Orthogonal array ($A_3B_2C_1D_3$)	Grey theory prediction design ($A_1B_3C_1D_3$)	Improvement rate
SiNW length (μm)	15.08	23.07	52.9 %
SiNW diameter (nm)	76.77	66.65	13.2 %

phonon mode (2TA), respectively (Yu et al. 1998). Compared with bulk crystal Si, the SiNW array has high Raman intensity (Fig. 7a). This increased intensity is probably due to the enhancement of transmitted excitation. The Raman peak of the SiNW arrays in (Fig. 7b) shows a downshift and asymmetrical broadening, which is attributable to the effect of phonon quantum confinement and the intensity enhancement, compared with that of bulk crystal Si.

Water contact angle (WCA) analysis is sensitive to the chemical composition of the topmost molecular layer and is a relatively simple, inexpensive and popular technique for the characterization of material

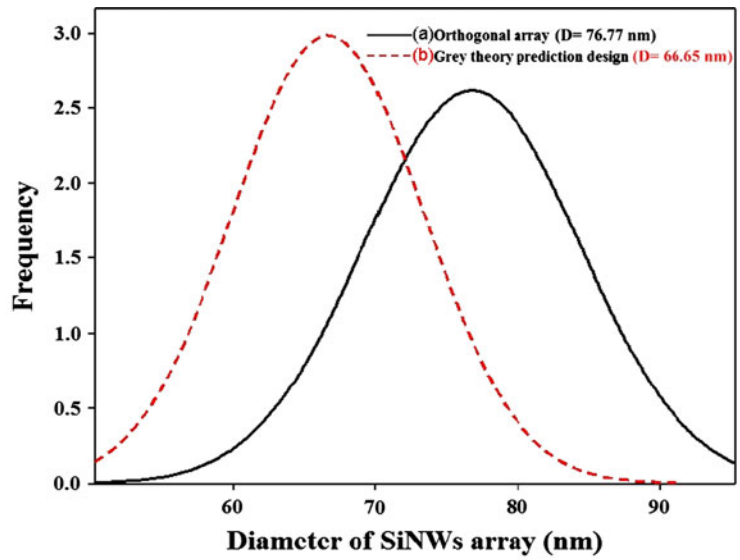

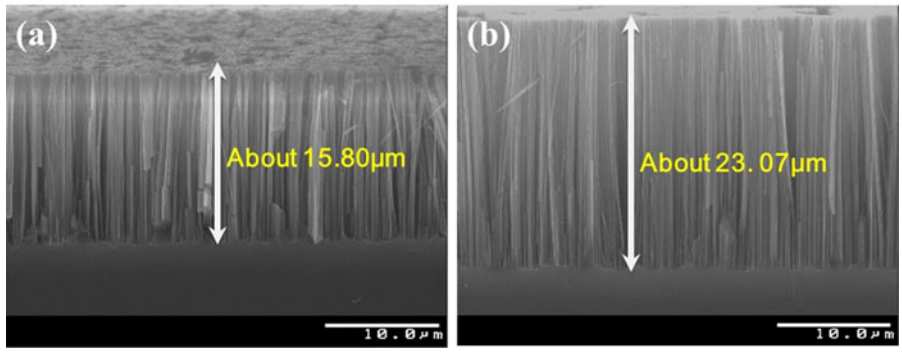

Fig. 4 Diameter and length of the SiNW arrays, using **a** orthogonal array parameters and **b** grey theory prediction design

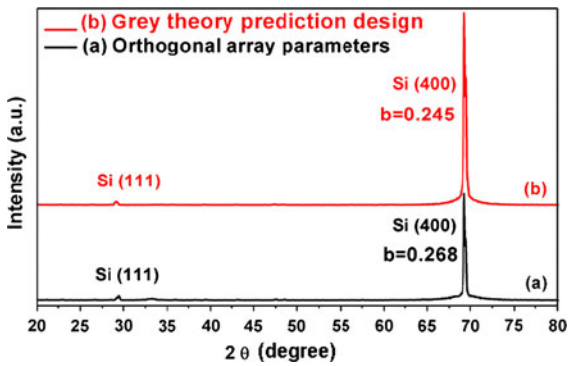

Fig. 5 X-ray diffraction spectrum for the SiNW arrays, using *a* orthogonal array parameters and *b* grey theory prediction design (*b*: full width at half maximum, FWHM)

surfaces. Figure 8 shows the WCA for the SiNW arrays, with and without the HF treatments. The SiNW arrays treated with HNO_3 have super-hydrophilic features, with a contact angle of 5.9 (Fig. 8a). After HF treatment, the SiNW arrays develop hydrophobic characteristics (WCA = 130.2°), due to the formation of Si-H_x groups at the surface of the SiNW arrays (Fig. 8b).

Figure 9 shows the FTIR spectra for the SiNW arrays with HNO_3 and HF treatment. The peak at 620 cm^{-1} is attributed to the Si–Si rocking vibration. The other peak at 1,100–1,250 cm^{-1} is attributed to the Si–O-Si stretching vibration. After HF treatment, the stronger Si–H asymmetric stretching mode bands at 2,245 cm^{-1} are observed (Fig. 9a). The use of HF induces Si-H_x bonds onto the surface of the SiNW arrays, which is confirmed by WCA analysis (hydrophobic characteristics). Before HF treatment, the signals from the Si–O bonds are much stronger (Fig. 9b), which indicates super-hydrophilic characteristics.

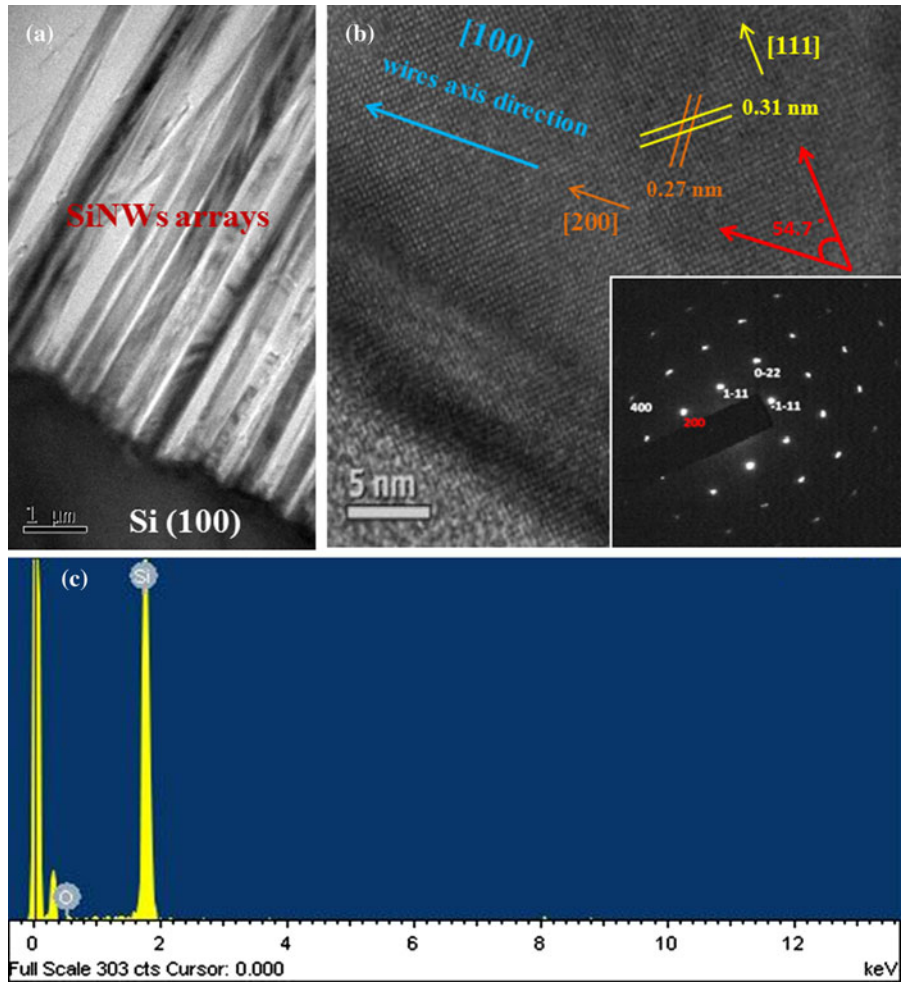

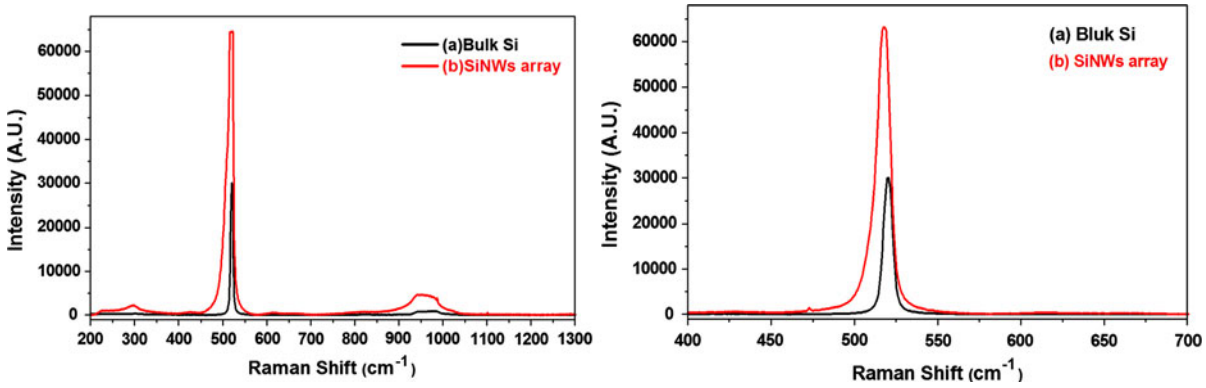

Fig. 6 TEM analysis of SiNW arrays for the grey theory prediction design sample: **a** typical TEM images, **b** HRTEM and **c** EDS analysis

Fig. 7 Raman analysis of the SiNW arrays at a concentration ratio for $AgNO_3$/HF of 0.02 M:13.8 M at 75 °C: *a* Raman spectra scan from 200 to 1,200 cm^{-1}; *b* partial view of the local curve in (*a*)

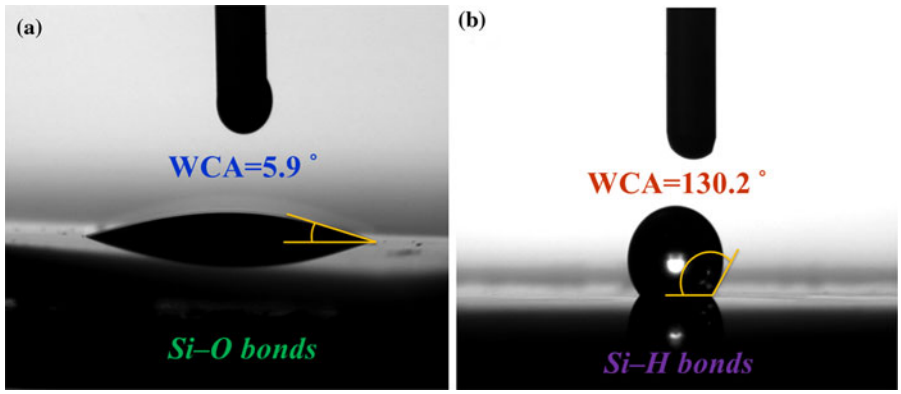

Fig. 8 Water contact angle (WCA) of the SiNW arrays: **a** treated with HNO_3 (WCA = 5.9°) and **b** treated with HF (WCA = 130.2°)

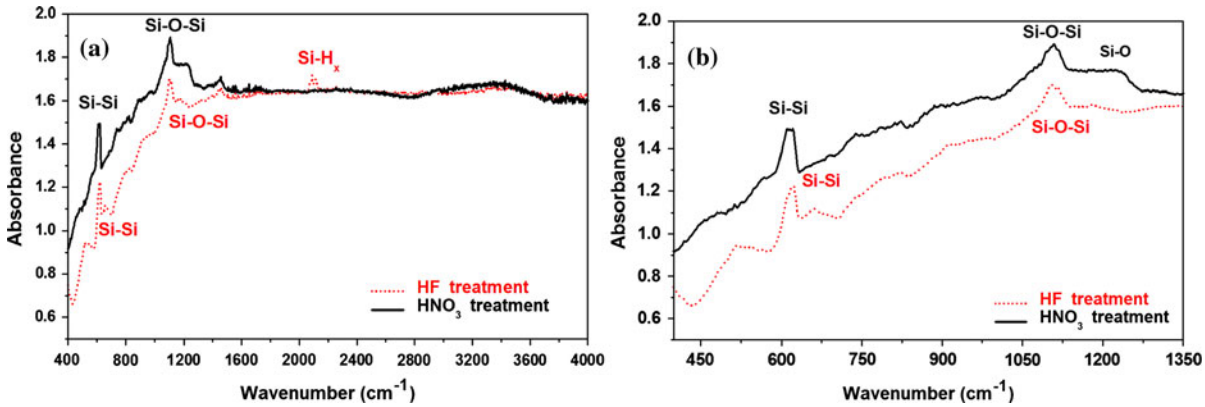

Fig. 9 FTIR analysis of the SiNW treated with HNO_3 and HF: **a** FTIR spectra scan from 400 to 4,000 cm^{-1}; **b** partial view of the local curve in (**a**)

The effect of etching time and solution temperature

The influence of etching time and solution temperature on the length of the SiNW arrays was investigated. The $AgNO_3$ concentration and HF concentration were maintained at 0.02 and 13.8 M, respectively. Figure 10 shows the SEM images of the SiNW arrays, which are straight and grow vertically on the Si substrates. According to dynamic theory, the linear relationship of the SiNW arrays can be adjusted by controlling the etching time and solution temperature. It can be seen that the length of SiNW arrays increases from 23.07 to 35.73 μm, when the etching time is increased from 15 to 45 min (Fig. 10 a, b and c). The length of the SiNW arrays increases from 14.33 to 23.07 μm, when the solution temperature is increased from 25 to 75 °C (Fig. 10 d, e and f). The conglomeration at the tips of the SiNWs array increases as etching time increases, because of the strong force or a Van der Waals interaction (Lee et al. 2006).

Conclusion

In this study, the use of electroless Ag-assisted etching (EAAE), using an aqueous HF solution containing $AgNO_3$, to produce oriented single-crystalline SiNW arrays on Si substrates is proven to be a simple, efficient and low cost method to prepare high quality of SiNW arrays. An L_9 (3^4) orthogonal array was used, with grey relational analysis, to optimize the SiNW arrays, using multiple performance characteristics. The major variable affecting the SiNW length is HF concentration (55.6 %). With a higher HF concentration, the SiNWs' growth is increased because of the ability of HF to dissolve oxides. By applying grey relational analysis in the confirmation runs, the SiNW arrays produced using

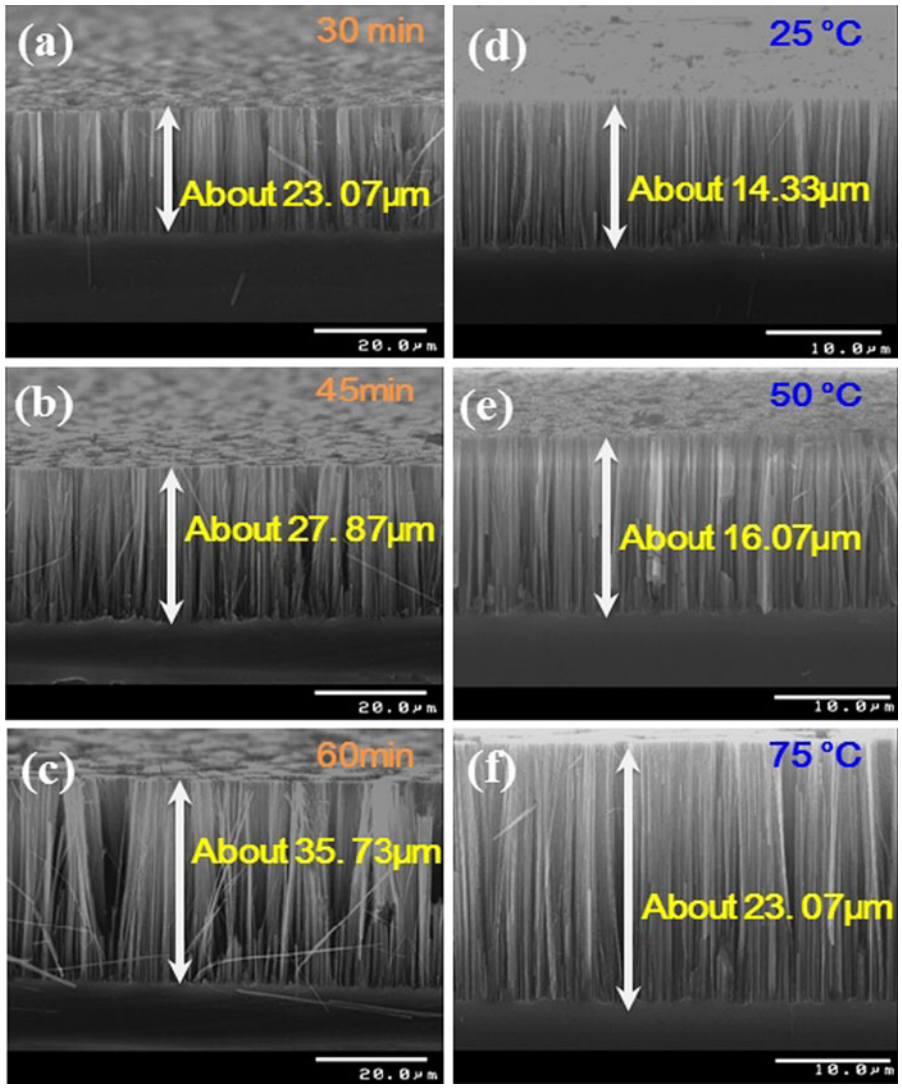

Fig. 10 SEM images of the SiNW arrays with etching times from 15 to 45 min (**a**, **b** and **c**) and solution temperatures from 25 to 75 °C (**d**, **e** and **f**), with a $AgNO_3$ concentration of 0.02 M and a HF concentration of 13.8 M

the grey theory prediction design with the orthogonal array parameters demonstrate an increase in the length of the SiNW array from 15.80 to 23.07 μm and a reduction in the average diameter of the SiNW array from 76.77 to 66.65 nm. By applying grey theory prediction design, it is seen that the intensity of the (400) diffraction peak becomes greater. The FWHM decreases from 0.268 to 0.245, which indicates that the crystallinity of the SiNW arrays can be improved. The SiNW arrays with HNO_3 treatment have super-hydrophilic features. After HF treatment, the SiNW arrays develop hydrophobic characteristics, due to the formation of Si-H_x groups at the surface of the SiNW arrays. Further, the linear relationship for the SiNW arrays can be adjusted by increasing the etching time (from 15 to 45 min) and the solution temperature (from 25 to 75 °C). The large area SiNW arrays have potential applications in interconnect, bio-technology and optoelectronic devices.

Acknowledgments The authors would like to thank the National Nano Device Laboratories (NDL99-C03S-041 and NDL99-C03S-042) and the National Science Council of the Republic of China, Taiwan for financially supporting this research, under Contract No. NSC 99-2221-E-009-031-MY2.

References

Alamdari R, Hajimirsadeghi S, Kohsari I (2010) Synthesis of silver chromate nanoparticles: parameter optimization using Taguchi design. Inorg Mat 46(1):60–64

Bandaru PR, Pichanusakorn P (2010) An outline of the synthesis and properties of silicon nanowires. Semicond Sci Tech 25:024003 (16 pp)

Chen DY, Hsu CY (2008) Growth of Ga-doped ZnO films with ZnO buffer layer by sputtering at room temperature. Superlattices Microstruct 44:742–753

Deng JL (1989) Introduction to grey system. J Grey Syst 1(1):1–24

Deng JL (1990) A course on grey system theory. HUST Press, Wuhan

Elfström N, Juhasz R, Sychugov I, Engfeldt T, Karlström AE, Linnros J (2007) Surface charge sensitivity of silicon nanowires: size dependence. Nano Lett 7(9):2608–2612

He Y, Fan CH, Lee ST (2010) Silicon nanostructures for bioapplications. Nano Today 5:282–295

Hsu CY, Tsang CH (2008) Effects of ZnO buffer layer on the optoelectronic performances of GZO films. Sol Energy Mater Sol Cells 92:530–536

Kern W, Puotinen DA (1970) Cleaning solutions based on hydrogen peroxide for use in silicon semiconductor technology. RCA Rev 31:187–206

Kim KD, Choi DW, Choa YH, Kim HT (2007) Optimization of parameters for the synthesis of zinc oxide nanoparticles by taguchi robust design method. Colloids Surf A Physicochem Eng Asp 311:170–173

Lee SJ, Morrill AR, Moskovits M (2006) Hot spots in silver nanowire bundles for surface-enhanced Raman spectroscopy. J Am Chem Soc 128(7):2200–2201

Liu WL, Hsieh SH, Chen WJ, Lee JH (2007) Study of nanosized Zinc oxide on Cu–Zn alloy substrate using Taguchi method. Surf Coat Technol 201:9238–9242

Lyons DM, Ryan KM, Morris MA, Holmes JD (2002) Tailoring the optical properties of silicon nanowire arrays through strain. Nano Lett 2(8):811–816

Ma DDD, Lee CS, Au FCK, Tong SY, Lee ST (2003) Small-diameter silicon nanowire surfaces. Science 299:1874–1877

Peng KQ, Lee ST (2011) Silicon nanowires for photovoltaic solar energy conversion. Adv Mater 23:198–215

Peng K, Zhu J (2003) Simultaneous gold deposition and formation of silicon nanowire arrays. J Electroanal Chem 558:35–39

Peng K, Yan Y, Gao S, Zhu J (2003) Dendrite-assisted growth of silicon nanowires in electroless metal deposition. Adv Funct Mater 13(2):127–132

Peng KQ, Huang ZP, Zhu J (2004) Fabrication of large area silicon nanowires p—n junction diode arrays. Adv Mater 16:73–76

Peng KQ, Wang X, Lee ST (2009a) Gas sensing properties of single crystalline porous silicon nanowires. Appl Phys Lett 95:243112 (3 pp)

Peng KQ, Wang X, Wu XL, Lee ST (2009b) Fabrication and photovoltaic property of ordered macroporous silicon. Appl Phys Lett 95:143119 (3 pp)

Peng KQ, Wang X, Wu XL, Lee ST (2009c) Platinum nanoparticle decorated silicon nanowires for efficient solar energy conversion. Nano Lett 9:3704–3709

Shao MW, Ma DDD, Lee ST (2010) Silicon nanowires: synthesis, properties and applications. Eur J Inorg Chem 27:4264–4278

Su C, Yeh C (2011) Optimization of the Cu wire bonding process for IC assembly using Taguchi methods. Microelectron Reliab 53:53–59

Taguchi G (1990) Introduction to quality engineering. Asian Productivity Organization, Tokyo

Teo BK, Sun XH (2007) Silicon-based low-dimensional nanomaterials and nanodevices. Chem Rev 107:1454–1532

Yu DP, Bai ZG, Ding Y, Hang QL, Zhang HZ, Feng SQ (1998) Silicon nano-wires synthesized using simple physical evaporation. Appl Phys Letters 72(26):3458–3460